TARP Subtypes Differentially and Dose-Dependently Control Synaptic AMPA Receptor Gating

Aaron D. Milstein[1,2,3,4], **Wei Zhou**[1,2,5], **Siavash Karimzadegan**[3,6], **David S. Bredt**[3,7], and **Roger A. Nicoll**[2,3,*]

[2]Department of Cellular and Molecular Pharmacology, University of California, San Francisco, CA 94143

[3]Department of Physiology, University of California, San Francisco, CA 94143

[4]Neuroscience Graduate Program, University of California, San Francisco, CA 94143

Summary

A family of transmembrane AMPA receptor regulatory proteins (TARPs) profoundly affects the trafficking and gating of AMPA receptors (AMPARs). Although TARP subtypes are differentially expressed throughout the CNS, it is unclear if this imparts functional diversity to AMPARs in distinct neuronal populations. Here we examine the effects of each TARP subtype on the kinetics of AMPAR gating in heterologous cells and in neurons. We report a striking heterogeneity in the effects of TARP subtypes on AMPAR deactivation and desensitization, which we demonstrate controls the time course of synaptic transmission. In addition, we find that some TARP subtypes dramatically slow AMPAR activation kinetics. Synaptic AMPAR kinetics also depend on TARP expression level, suggesting a variable TARP/AMPAR stoichiometry. Analysis of quantal synaptic transmission in a TARP γ-4 knockout (KO) mouse corroborates our expression data and demonstrates that TARP subtype-specific gating of AMPARs contributes to the kinetics of native AMPARs at central synapses.

Introduction

The encoding and processing of information in the brain depends on the strength and timing of synaptic signaling. The predominant mechanism for fast excitatory synaptic transmission in the mammalian central nervous system is the depolarization of the postsynaptic membrane by the AMPA receptor (AMPAR) family of glutamate-gated ion channels. The size of AMPAR-mediated synaptic currents is primarily determined by the peak concentration of glutamate in the synaptic cleft, the number of postsynaptic AMPARs and their inherent affinity for glutamate (Bredt and Nicoll, 2003; Clements, 1996; Kullmann et

*Address correspondence to: Roger A. Nicoll, Dept. of Cellular and Molecular Pharmacology, University of California, San Francisco, CA 94143, nicoll@cmp.ucsf.edu, Phone: (415) 476-2018.
[1]These authors contributed equally to this work
[5]SRI international, LA150 Menlo Park, CA, 94025,
[6]Program in Neurobiology & Behavior, Columbia University, New York, NY 10032,
[7]Lilly Research Laboratories, Corporate Center, Indianapolis, IN 46285

al., 1999). In contrast, the shape of synaptic currents is governed by diverse processes, including the rate of glutamate clearance (Barbour and Hausser, 1997; Diamond, 2001; Overstreet et al., 1999; Sargent et al., 2005), the ultrastructure of the surrounding neuropil (Cathala et al., 2005; Xu-Friedman and Regehr, 2003) and the gating kinetics of AMPARs. The biophysical properties of synaptic AMPAR complexes depend on their molecular identity, with contributions from subunit composition, splice variation, RNA editing and posttranslational modification (Jonas, 2000; Koike et al., 2000; Mosbacher et al., 1994; Swanson et al., 1997). The mechanisms that govern the trafficking and gating of synaptic AMPARs are of particular interest given accumulating evidence that activity-dependent regulation of these processes provides a molecular basis for learning and memory (Bredt and Nicoll, 2003; Malinow and Malenka, 2002; Sheng and Kim, 2002)

AMPARs are composed of heterotetrameric combinations of the subunits GluR1–4. In addition to these pore-forming subunits, neuronal AMPAR complexes also contain auxiliary subunits that regulate receptor trafficking and gating (Nicoll et al., 2006; Osten and Stern-Bach, 2006; Ziff, 2007). This family of transmembrane AMPAR regulatory proteins (TARPs) consists of its prototypical member, stargazin (γ-2), and the homologous γ-3, γ-4 and γ-8. Loss of γ-2 causes profound deficits in surface and synaptic AMPAR expression in cerebellar granule neurons (Hashimoto et al., 1999) and loss of γ-8 impairs AMPAR expression in hippocampal pyramidal neurons (Fukaya et al., 2006; Rouach et al., 2005). It has been hypothesized, but not rigorously tested, that overlapping expression of other TARP subtypes in most neurons functionally compensate for one another (Fukaya et al., 2005; Tomita et al., 2003). TARPs were originally identified and discriminated from the homologous proteins γ-1 and γ-5 based on their ability to rescue the surface expression of native AMPARs in cultured cerebellar granule neurons from *stargazer* mutant mice (Tomita et al., 2003). However, it remains untested whether other TARP subtypes share the roles of γ-2 in targeting AMPARs to synapses and modulating their channel properties (Chen et al., 2000; Tomita et al., 2005).

Therefore, we assessed the roles of each TARP subtype on synaptic targeting and channel gating of AMPARs by performing electrophysiological recordings in two model systems: human embryonic kidney (HEK293T) cells and *stargazer* cerebellar granule neurons. By rapidly applying glutamate to outside-out patches from HEK293T cells expressing AMPARs and TARPs, we determined that TARP subtypes (γ-2, γ-3, γ-4 and γ-8) differentially regulate the rates of activation, deactivation and desensitization of AMPARs. Recordings of quantal synaptic AMPAR currents in *stargazer* granule cells demonstrate that all TARP subtypes are sufficient to traffic AMPARs to synapses. Furthermore, the time course of rise and decay of AMPAR-mediated synaptic currents depends on the subtype of associated TARP, and these functional differences among TARP family members can be attributed to differences in their first extracellular domain. Finally, we demonstrate that control of synaptic AMPAR gating by TARPs depends on the level of TARP expression, suggesting that the number of TARP molecules associated with individual AMPAR complexes is not fixed.

Results

TARP Subtype Determines the Kinetics of AMPA Receptors in Heterologous Cells

The key determinant that shapes most excitatory synaptic currents is the rapid deactivation of AMPARs, which reflects a change in the conformational state of the receptors and their subsequent unbinding of glutamate (Jonas, 2000; Takahashi, 2005). At some synapses, however, persistent agonist exposure drives AMPARs into a distinct closed bound conformation, a process referred to as desensitization (Raman and Trussell, 1995). Having previously shown that TARP γ-2 slows the time courses of both deactivation and

desensitization (Priel et al., 2005; Tomita et al., 2005), we sought to determine if other TARP subtypes also modulate the kinetics of AMPARs. The AMPAR subunit GluR1 (flip) was expressed in HEK293T cells with or without individual TARPs. Currents from outside-out patches were recorded in response to either 1 ms or 100 ms applications of glutamate to measure deactivation and desensitization, respectively. Each TARP isoform prolonged deactivation and desensitization of GluR1 (Figures 1A and 1B), though the magnitude of the effect varied greatly among TARP subtypes; γ-4 and γ-8 affected deactivation most dramatically (Figures 1A and 1C) and γ-8 had the largest effect on desensitization (Figures 1B and 1D). For simplicity, the decay times portrayed here represent weighted time constants calculated from the area under the peak-normalized response (Cathala et al., 2005) (see Experimental Procedures). However, currents were best fit by a sum of two exponential components (see Table S1 in the Supplemental Data available online), which reveal that the effect of TARPs on AMPAR currents is primarily to promote a slow component of decay. These results are consistent with a recent report that TARP γ-4 modulates AMPAR desensitization more effectively than γ-2 (Korber et al., 2007). In conducting these experiments, we also observed an unexpected effect of TARPs on the activation kinetics of GluR1; γ-4 and γ-8 prolonged the rise time in response to 1 ms applications of glutamate nearly two-fold (Figure 1E). These results demonstrate that the kinetic regulation of AMPARs by TARPs depends on TARP subtype.

TARP Subtype Shapes Quantal Synaptic AMPAR Currents

To compare the above findings to neuronal receptors and determine the effects of TARPs on the synaptic targeting of AMPARs, we performed whole-cell voltage-clamp recordings on dissociated cerebellar granule neurons in cultures from *stargazer* mice. This model system has two essential features: 1) the small cell body and electrotonically compact dendritic arbors of cerebellar granule neurons allow for accurate somatic measurement of the time course of synaptic currents (Cathala et al., 2005; Silver et al., 1996); and 2) *stargazer* cerebellar granule neurons lack functional TARPs but contain an intracellular pool of native AMPARs that can be recruited to surface and synaptic membranes by ectopic TARP expression (Chen et al., 2000; Tomita et al., 2003). This "clean" background contrasts with hippocampal pyramidal neurons, which contain expansive dendrites that extensively filter synaptic conductances (Magee and Cook, 2000), and which express multiple TARP isoforms (Tomita et al., 2003).

In *stargazer* granule neurons, local perfusion of agonist fails to evoke a significant AMPAR response (Chen et al., 2000; Tomita et al., 2003) (Figure 2). However, neurons transiently transfected with TARPs exhibit robust whole-cell responses to glutamate comparable in amplitude to those in wild type neurons (Chen et al., 2000; Tomita et al., 2003) (Figure 2). This strongly suggests that TARPs are expressed at saturating levels and that all available AMPARs are being delivered to the surface (see Experimental Procedures). In the presence of TTX, brief local applications of hypertonic sucrose solution evoked asynchronous release of single vesicles of glutamate from the presynaptic terminals of nearby granule neurons. Resulting AMPAR miniature excitatory postsynaptic currents (mEPSCs) were readily detected in neurons expressing each of the TARPs γ-2, γ-3, γ-4 and γ-8, but not in untransfected neurons (Figure 3A). This demonstrates that each TARP is sufficient for localizing AMPARs at synapses. Notably, the average peak amplitude of the "rescued" mEPSCs varied among TARPs (γ-3: ~10% increase relative to γ-2; γ-8: ~20% decrease relative to γ-2; see Figure 3B). Since each TARP rescued surface AMPAR responses to the same extent (Figure 2), these differences in the size of mEPSCs must either reflect differences in gating, or in the ability of different TARPs to target AMPARs to synapses.

To determine the effects of each TARP subtype on synaptic AMPAR gating, we measured the rise and decay kinetics of the recorded mEPSCs. Examination of the sample records

(Figure 3A) clearly shows that the duration of mEPSCs varies dramatically depending on the subtype of TARP expressed. This difference is shown more clearly in the expanded records in Figures 3C and 3D, in which average mEPSCs from individual cells are displayed in grey and the averages of all experiments for each condition are displayed in color. The decay of mEPSCs rescued with γ-3 was slightly, but significantly, faster than γ-2, whereas mEPSCs mediated by γ-8 decayed similarly to γ-2. In striking contrast, the mEPSCs rescued with γ-4 were dramatically slower than γ-2 (Figures 3A–3D). As with the patch data, decay times reflect a weighted decay measure (see Experimental Procedures). A detailed analysis of double exponential fits to the mEPSC data is presented in Table S2 in the Supplementary Data available online. Close examination of mEPSC rise times also reveals differences among the various TARPs (Figure 3E), corroborating the aforementioned effect on activation kinetics observed in HEK293T cells. That the effects of γ-3 and γ-8 relative to γ-2 differ in granule neurons as compared to heterologously expressed GluR1 suggests a contribution from AMPAR subunit composition in the control of channel gating by TARPs, as recently reported (Kott et al., 2007).

TARPs Dose-Dependently Control Synaptic AMPAR Gating

In *stargazer* heterozygote (+/*stg*) neurons, whole-cell AMPAR-mediated responses to glutamate were reduced by half compared to wild type (Figure 2) and the amplitudes of mEPSCs were also clearly reduced (Figures 4A and 4B), consistent with a model in which the expression level of TARP is limiting for the delivery of AMPARs to the surface and synaptic membranes. Unexpectedly, overexpression of γ-2 in *stg*/*stg* granule neurons resulted in mEPSCs that were dramatically slowed compared to wild type neurons (Figures 4C and 4D), which only express TARP γ-2. Expression of γ-2 in wild type neurons also slowed AMPAR mEPSCs to a similar extent (data not shown), ruling out the possibility of some deficit in synapse formation or maintenance in *stg*/*stg* neurons. Furthermore, mEPSCs in +/*stg* neurons were slightly but significantly faster than wild type (Figures 4C and 4D). These differences are particularly evident when comparing the values obtained from fitting average mEPSCs with a double exponential function (see Table S2 in the Supplementary Data available online). Differences in rise time in these experiments were small (Figure 4E).

Given that AMPARs in granule neurons absolutely require TARP association for surface and synaptic localization (Chen et al., 2000; Hashimoto et al., 1999), what mediates this dependence of AMPAR kinetics on TARP expression level? One interesting possibility is that individual AMPAR complexes can associate with more than one TARP molecule, depending on the availability of TARP. Accordingly, the relative expression level of TARP and AMPAR in neurons determines the number of TARPs associated with single AMPAR complexes, which in turn influences synaptic AMPAR gating and the time course of synaptic transmission. Alternatively, increased expression levels of TARPs could selectively traffic different populations of AMPARs with intrinsically different kinetics. Indeed, a recent report demonstrated that flop splice variants of AMPARs contain an ER retention signal that reduces their surface expression compared to flip splice variants in heterologous cells (Coleman et al., 2006). In that study, the surface delivery of flop AMPAR subunits could be facilitated by co-expression either with flip AMPAR subunits, or with TARP γ-2. In order to test the possibility that differences in the relative surface expression levels of flip and flop AMPAR splice variants mediates the differences in AMPAR gating observed in Figure 4, we conducted a functional assay of AMPAR splice variation using pharmacology. While cyclothiazide (CTZ) reduces desensitization and potentiates peak glutamate responses selectively on flip AMPARs, 4-[2-(phenylsulfonylamino)-ethylthio]-2,6-difluoro-phenoxyacetamide (PEPA) acts selectively on flop AMPARs. These drugs have previously been used to detect relative differences in the expression of flip and flop AMPARs in distinct neuronal populations (Sekiguchi et al., 1998). We recorded whole-cell responses to

glutamate in cultured granule neurons, first in the presence of CTZ, and then in the presence of PEPA, and calculated PEPA/CTZ ratios from the resulting current amplitudes (see Figure S1 in the Supplementary Data available online). This ratio was near unity, indicating substantial contributions from both flip and flop AMPARs, and did not differ between wild type, +/*stg* and γ-2 in *stg/stg*. Therefore, the dependence of synaptic AMPAR kinetics on TARP expression level does not reflect differences in the surface expression of distinct AMPAR splice variants. Rather, these data favor the hypothesis that AMPARs associate with TARPs with a variable stoichiometry. Further studies in heterologous systems as well as detailed structural analyses of TARP/AMPAR interactions will likely be required to validate this possibility.

TARP Subtype and Expression Level Control AMPAR Agonist Affinity

To determine how the various TARPs differentially modulate AMPAR channel kinetics, we examined the effect of TARP subtype on the apparent affinity for agonist in granule cells. We recorded whole-cell responses to the local application of various concentrations of the nondesensitizing agonist kainate. A typical experiment is shown in Figure 5A, and the resulting dose-response relationships are shown in Figures 5B and 5C. The kainate EC_{50} values for surface AMPARs depends on the subtype of associated TARP (see Figure 5B and Table S3 in the Supplemental Data available online). These values correlate closely with the effects of each TARP on mEPSC decay – the faster decay of AMPARs associated with γ-3 is coupled with a higher kainate EC_{50}, while the slower decay mediated by γ-4 is coupled with a lower EC_{50}. It is worth noting that the peak responses to saturating kainate (3 mM) did not differ significantly between TARPs (see Table S3 in the Supplemental Data available online), suggesting that previously reported differences between TARPs in the ratio of kainate to glutamate responses measured at steady-state with subsaturating agonist concentrations (Tomita et al., 2005) likely reflect multiple processes, including relative differences in the apparent affinity of AMPARs for kainate, and the degree of steady-state desensitization in response to glutamate. Furthermore, TARP γ-4 significantly reduced the Hill coefficient calculated from the shape of the kainate dose-response relationship (see Table S3 in the Supplemental Data available online). This effect of TARPs has also been reported in heterologous systems (Priel et al., 2005; Tomita et al., 2005) and may indicate that TARPs reduce the number of agonist molecules that must be bound to effectively open the AMPAR channel.

The apparent affinity of these native AMPARs for agonist also depended on the expression level of TARP γ-2 (Figure 5C), with differences in kainate EC_{50} again corresponding to differences in mEPSC decay for wild type, +/*stg* and γ-2-expressing *stg/stg* neurons. Notably, overexpression of γ-2 also resulted in a substantial increase in the peak response to saturating kainate relative to wild type (see Table S3 in the Supplemental Data available online), indicating that the potency of this partial agonist is also TARP dose-dependent.

TARP Subtype-Specific Gating of AMPARs Depends on a TARP Extracellular Domain

Given the profound differences in kinetics observed for mEPSCs rescued with the various TARPs, we sought to determine the molecular mechanism for TARP subtype-specific control of AMPAR gating. Previous studies using chimeras between γ-2 and the inactive homologue γ-5 demonstrated that the first extracellular domain (Ex1) of γ-2 is important for its effects on AMPAR gating and pharmacology (Tomita et al., 2005). We therefore generated a series of chimeras in which the Ex1 domains of distinct TARP subtypes were exchanged. Specifically, we replaced the Ex1 domain of γ-2 with that of γ-4 (γ-2×4) and visa versa (γ-4×2), and replaced the Ex1 domain of γ-3 with that of γ-8 (γ-3×8) and visa versa (γ-8×3). All four of these chimeric TARPs rescued surface AMPAR responses (data not shown) as well as AMPAR mEPSCs in *stargazer* granule neurons (Figure 6A). mEPSCs

mediated by γ-2×4 displayed the slow decay kinetics normally associated with γ-4, while γ-4×2 produced the fast decay kinetics associated with γ-2 (Figures 6C and 6D). Remarkably, differences in the rise kinetics of AMPARs imparted by γ-2 and γ-4 were also reversed by replacement of this Ex1 domain (Figure 6E). While mEPSC amplitudes did not differ between γ-2 and γ-4 (see Figures 3A and 3B), they did for γ-2×4 and γ-4×2 (Figures 6A and 6B). This agrees with previous work demonstrating that the Ex1 domain can influence the peak amplitude of synaptic responses (Tomita et al., 2005). The rise and decay phenotypes of TARPs γ-3 and γ-8 were also reversed for the chimeras γ-3×8 and γ-8×3. Although the weighted decay constant is similar for γ-2×4 and γ-3×8 (Figures 6C and 6D), the time course and relative contribution of a slow component of decay are different, suggesting subtle differences in the mechanisms by which these Ex1 domains influence AMPAR kinetics. These results indicate that Ex1 is a critical determinant of TARP subtype-specific gating of AMPARs.

Modeling the Kinetic Regulation of AMPARs by TARPs

We were intrigued by the evident sufficiency of a single TARP extracellular domain for the TARP subtype-specific control of AMPAR channel kinetics, so we employed a mathematical model to gain insight into the underlying mechanisms. We modified a recently proposed kinetic scheme (Zhang et al., 2006) (depicted in Figure 7A) and used a least square error optimization algorithm to fit our deactivation and desensitization data from GluR1 patches with and without TARPs. The following experimental observations placed limits on the model's transition rates: 1) TARPs increase agonist affinity, but do not appear to slow agonist unbinding (Turetsky et al., 2005); 2) TARPs increase the rate of recovery from desensitization (Priel et al., 2005; Turetsky et al., 2005); 3) TARPs increase channel opening probability during prolonged agonist application without changing open times (Tomita et al., 2005); and 4) TARPs slow current decay by increasing the relative contribution and time course of a slow component of decay (Zhang et al., 2006) (this study). The resulting simulated responses to 1 ms or 100 ms square pulses of 1 mM glutamate for GluR1 alone, GluR1 + γ-2, and GluR1 + γ-4 are shown in Figures 7B – 7D. The fitted rate constants and calculated time constants of deactivation, desensitization and rise are provided in Table 1. Comparison to the experimental data in Figures 1A – 1E shows that our model predicts well these features of AMPARs and their differential control by TARPs γ-2 and γ-4.

What does this model tell us about the actions of TARPs on AMPARs? As shown in Figure 7A, before the glutamate-bound receptor, RG, can open, a structural rearrangement of the ligand-binding domain must occur. This "cleft closure" step allows the receptor to "trap" glutamate in a state from which it cannot readily unbind, denoted C_1. Both channel opening and desensitization can occur from this "closed cleft" conformation. To account for the multiple exponential components of decay displayed by the AMPAR when associated with TARPs, this model also includes a second closed state C_2 that results from a presumed conformational shift from C_1. The parameters that result from fitting this model to our data (see Table 1) indicate that the primary effect of TARP association is to stabilize the closed-bound conformations C_1 and C_2 by altering the rates in and out of these states. While the closed conformation C_2 is extremely unstable (fast CS_{-1}) and rarely populated (slow CS_{+1}) in the absence of TARP, association with TARP stabilizes this conformation of the receptor (decreases CS_{-1}) and increases its relative occupancy (increases CS_{+1}). Accordingly, γ-4 effects these changes to a greater degree than γ-2, which corresponds to their relative difference in slowing AMPAR decay. Furthermore, these simple rate changes also fully account for the effect of γ-4 on AMPAR activation (see Figure 7D). By increasing the number of channels that sequentially pass through the closed states C_1 and C_2 before opening, γ-4 prolongs the latency before channels open after binding glutamate, which slows the time to peak response. Although our previous study suggested that a simple increase in

the channel opening rate, β, could fully account for the effects of TARPs on AMPAR kinetics (Tomita et al., 2005), within the current framework, increasing β leads to a speeding of activation kinetics. However, it is important to note that stabilizing the closed state C_2 does increase the probability of opening at steady-state since β is large compared to the other rates away from this state. A simple decrease in the unbinding rate of glutamate, k_{-1}, was also not sufficient to account for our data.

TARP Subtype-Specific Gating of AMPARs Contributes to Endogenous AMPAR Kinetics at a Central Synapse

Given the dramatically slow mEPSCs observed in *stargazer* cerebellar granule cells overexpressing TARP γ-4, and the dependence of AMPAR gating on TARP expression level, we wondered whether endogenous γ-4 confers slow kinetics to synaptic AMPARs in the brain. To address this, we generated a γ-4 knockout (−/−) mouse by disrupting the γ-4 gene through homologous recombination in embryonic stem cells (see Figures S2A and S2B in the Supplemental Data available online). Immunoprecipitation of brain protein extracts with a γ-4-selective antibody and subsequent western blot analysis confirmed that γ-4 protein was absent in γ-4 −/− mice (see Figure S2C in the Supplemental Data available online). Immunohistochemical staining of sagittal sections of brain for GluR1 and GluR2/3 showed no obvious difference between γ-4 −/− and wild type mice (data not shown). γ-4 is expressed transiently throughout the developing brain, with especially high levels in the striatum (Fukaya et al., 2005; Tomita et al., 2003). Therefore, we initially recorded quantal synaptic AMPAR currents from medium spiny neurons (MSNs) in the dorsolateral striatum of neonatal animals (P5–P6). mEPSC amplitudes were reduced in γ-4 −/− neurons as compared to wild type (Figure 8A and 8B), suggesting that this TARP normally participates in the synaptic targeting of AMPARs at this developmental stage. Furthermore, both the decay and rise time of mEPSCs were significantly faster in γ-4 −/− neurons (Figure 8C and 8D). This suggests that the remaining synaptic AMPARs are associated with other TARPs that do not slow the decay or rise of AMPARs to the same extent as γ-4. The effects of loss of γ-4 on synaptic AMPAR kinetics decline with age in parallel with the decreased expression of γ-4, as mEPSCs recorded from striatal neurons in γ-4 −/− and wild type mice at P14–P16 were identical (see Figure S3 in the Supplementary Data available online). Interestingly, although the loss of γ-4 accelerated mEPSC decay in young animals, mEPSCs in both genotypes slowed with age (compare Figures 8C and 8D with Figures S3C and S3D in the Supplementary Data available online). This developmental slowing of mEPSCs occurred in parallel with a decreasing input resistance (see Figure S4 in the Supplementary Data available online) and likely reflects increased filtering due to the elaboration of the dendritic tree (Magee and Cook, 2000) rather than changes in the channel properties of AMPARs. These results demonstrate that functional heterogeneity in the control of AMPAR gating by TARP subtypes must be considered in order to fully account for the kinetics of AMPARs in populations of neurons that differentially express multiple TARP isoforms.

Discussion

In this study we demonstrate a striking diversity in the regulation of the biophysical properties of AMPARs by TARP auxiliary subunits. We discovered unexpected differences in the control of AMPAR activation, deactivation and desensitization by TARP subtypes that were not predicted by previous analyses of steady-state currents in response to prolonged exposure to agonists (Kott et al., 2007; Tomita et al., 2005). We also provide the first demonstration that all TARP subtypes are sufficient to traffic AMPARs to synapses, and that their differential regulation of channel kinetics manifests in the shape of synaptic responses. Finally, we use a γ-4 knockout mouse to show that developmental regulation of TARP subtype expression contributes to the endogenous kinetics of synaptic AMPARs.

Importantly, the differential control of AMPAR decay by TARP subtypes is apparent for a variety of AMPAR subunit compositions, including heterologous GluR1 (flip) and native AMPARs in both cerebellar granule cells and striatal MSNs. Granule cells express predominantly heteromers of GluR2 and GluR4 (both flip and flop) (Mosbacher et al., 1994) and MSNs express heteromers of GluR1, GluR2 and GluR3 (Vorobjev et al., 2000). Consistent with a recent report that demonstrated contributions by AMPAR subunit composition to the regulation of AMPARs by TARPs (Kott et al., 2007), we observed subtle differences in the effects of the TARPs γ-3 and γ-8 on AMPARs in granule cells as compared to GluR1 homomers. We recently reported that γ-7 shares many characteristics of TARPs, including a slowing of AMPAR deactivation and desensitization (Kato et al., 2007). However, this TARP only rescued AMPAR surface currents in *stargazer* granule cells to a small extent. No synaptic currents could be detected in these experiments (n = 24, data not shown), so we were unable to further characterize the effect of this protein on AMPAR properties.

We also observed an unexpected effect of some TARP subtypes on the activation kinetics of AMPARs. While a relationship between agonist affinity and rise time is established for NMDA receptors (Lester and Jahr, 1992; Pan et al., 1993), the kinetics of AMPAR activation have received relatively little consideration (but see (Clements et al., 1998) due to two confounds: 1) AMPAR activation occurs rapidly, on the same time-scale as solution exchange in fast-application experiments (hundreds of microseconds); and 2) the rise times of mEPSCs recorded from neurons with extensive dendrites vary considerably depending on the distance of the activated synapse from the cell body (Magee and Cook, 2000). For these reasons, it is critical for our interpretation of the patch data that the same effects of TARPs γ-4 and γ-8 on AMPAR activation kinetics were also evident in recordings of mEPSCs from cultured cerebellar granule neurons, which have extremely short, electrotonically compact dendrites (Cathala et al., 2005; Silver et al., 1996).

Our experiments in *stargazer* cerebellar granule neurons revealed that neurons expressing low levels of TARP display mEPSCs with a rapid time course, and neurons expressing saturating levels of TARP exhibit mEPSCs that decay with a pronounced slow component. Although biochemical assays have not detected TARPs of more than one subtype associated with single AMPAR complexes (Tomita et al., 2003), a recent single-particle electron microscopy study detected at least two TARP intracellular domains associated with purified native AMPAR complexes (Nakagawa et al., 2005; Nakagawa, personal communication). The nature of the interaction between TARPs and AMPARs is not well understood, though it appears to involve extracellular as well as transmembrane and intracellular domains (Tomita et al., 2005; Tomita et al., 2004). Whether this interaction is permissive for more than two TARP molecules to associate with single AMPARs is unknown. Regardless of the actual stoichiometry of TARPs and AMPARs, our data suggests it can vary, depending on the availability of TARP. While minimal TARP binding appears sufficient to traffic AMPARs to the surface and to the synapse, incorporation of additional TARPs progressively increases agonist affinity and current decay. Interestingly, studies of other ion channels have shown that auxiliary subunits can regulate trafficking and gating separately and with differing dose-dependencies (Canti et al., 2001; Wang et al., 2002). Whether modulation of TARP expression level is a mechanism whereby neurons can acutely regulate synaptic transmission is unknown. However, it has been shown in a number of brain areas that the kinetics of AMPAR EPSCs undergo changes during postnatal development (Takahashi, 2005). Whereas this may reflect diverse mechanisms, ranging from changes in AMPAR subunit composition to changes in the time course of glutamate in the synaptic cleft (Cathala et al., 2005; Wall et al., 2002), our data suggest that changes in TARP subtype and TARP expression level could also contribute.

What processes underlie the complex kinetics of AMPARs and their regulation by TARP auxiliary subunits? Structural studies suggest that interactions between adjacent subunits within an AMPAR complex participate in conformational changes that follow agonist binding but precede channel opening (Hansen et al., 2007; Horning and Mayer, 2004; Sun et al., 2002). Accordingly, agonists of varying chemical structure differ in their ability to induce such changes in conformation (Armstrong and Gouaux, 2000). The kinetic model that we extend here was proposed by Zhang et al. to explain the behavior of four AMPAR agonists of varying affinity that produce profound differences in kinetics (Zhang et al., 2006). This model predicts that differences in the relative stabilities of multiple closed ligand-bound conformations of the receptor produce differences in affinity as well as deactivation and desensitization. Here we demonstrate that these same effects of TARPs on AMPAR gating, as well as the additional effects of slowing activation and speeding recovery from desensitization, are also well accounted for by changes in the rate constants between closed ligand-bound states of the receptor. As with any simple model, ours does not quantitatively describe certain aspects of AMPAR function, and other sets of rate constants could likely fit the data. Ultimately, accounting for multiple glutamate binding sites and multiple open states with varying conductance is needed to fully describe AMPAR single channel activity and the time course of recovery from desensitization (Robert et al., 2005; Robert and Howe, 2003). Nevertheless, our modeling provides a framework to understand how TARPs can allosterically modulate diverse properties of AMPARs.

What is the functional relevance of TARP subtype-specific control of AMPAR gating to synaptic transmission? To address this question, we focused on TARP γ-4, which caused the most dramatic effects on AMPAR kinetics in our expression systems. We genetically deleted γ-4 and analyzed synaptic transmission in MSNs in the striatum, which express high levels of γ-4. The rise and decay of AMPAR mEPSCs were significantly faster in γ-4 −/−, demonstrating its unique effects are pertinent at physiological expression levels. By slowing both the rise and decay phases of AMPAR EPSCs, γ-4 maximizes the total charge transfer through postsynaptic AMPARs in response to single vesicles of transmitter. Given that γ-4 is widely expressed in brain during early development, this TARP could play a role in the initial formation of synapses, possibly by providing neurons with a highly sensitive reporter of presynaptically released glutamate. However, as neurons mature, recruiting TARP/AMPAR complexes with faster decay kinetics to synapses may allow for the temporal precision required for neuronal circuit function (Hausser and Clark, 1997). Furthermore, the slow component of decay imparted to AMPARs by TARPs will likely influence the activation of synaptic NMDARs, which depend on local depolarization of the synaptic membrane (Kampa et al., 2004). In this manner, TARP subtypes could potentially influence the degree to which individual synapses can undergo activity-dependent changes in synaptic strength.

Taken together, the results presented here provide a clear demonstration that the TARP family of AMPAR auxiliary subunits confers a remarkable heterogeneity to the channel behavior of native AMPARs. Interestingly, recent studies have begun to uncover unexpected heterogeneity and synapse-specificity in the localization of the PSD-MAGUK proteins that cluster TARP/AMPAR complexes at synapses through a PDZ interaction (Bats et al., 2007; Beique et al., 2006; Chen et al., 2000; Elias et al., 2006; Schnell et al., 2002). Furthermore, AMPARs of varying subunit composition have been shown to be differentially trafficked to distal versus proximal synapses (Andrasfalvy et al., 2003). It will be of interest to determine if a similar synapse-specificity is displayed in the localization of individual TARP subtypes within neurons that express multiple TARP isoforms.

Experimental Procedures

Plasmid Constructs

cDNAs encoding rat γ-2, γ-3, γ-4 and γ-8 used in previous studies (Rouach et al., 2005; Tomita et al., 2003) were subcloned by PCR into the EcoR1 and Sal1 restriction sites of the vector pIR2-EGFP (Clontech) to allow for the coexpression of untagged TARP protein and EGFP via an internal ribosome entry site (IRES) under the control of a strong CMV promoter. In order to normalize the expression levels of each TARP subtype, a Kozak translational start sequence was engineered before the start codon in the cDNAs encoding each TARP. Transfected cells were detected by EGFP fluorescence, which was equivalent for each TARP subtype expressed. No correlations were found between apparent EGFP fluorescent intensity, whole-cell currents, or mEPSC amplitudes or decay times for any construct, suggesting that the ectopic TARP expression in neurons shown in this study reflects saturation with respect to the low endogenous expression of AMPARs in cultured cerebellar granule neurons. cDNA encoding rat GluR1 (flip) was subcloned by PCR into the EcoR1 and Sal1 restriction sites of a modified version of the vector pIR2 where the EGFP was replaced by the monomeric red fluorescent protein mCherry (Shaner et al., 2004) (originally acquired from Roger Tsien and subcloned by PCR into pIR2 by Susan Voglmaier). This allowed for the visual detection of HEK293T cells coexpressing GluR1-IRES-mCherry with TARP-IRES-EGFP.

Electrophysiology

Complete descriptions of the conditions whereby HEK293T and dissociated granule neurons were maintained in culture, as well as the solutions used for electrophysiological recordings, the systems used for local solution exchange and transfection procedures were provided in a recent report (Kato et al., 2007). Recordings were collected using an Axopatch 1D amplifier (Axon Instruments), filtered at 2 kHz, digitized using hardware from National Instruments, and analyzed online using custom software in Igor Pro (Wavemetrics). Outside-out patch recordings were sampled at 50 kHz, while all neuronal recordings were sampled at 10 kHz. While the extremely low noise in recordings from cultured granule cells allowed us to obtain good exponential fits to the raw data without further filtering, a binomial smoothing filter was applied to average currents from outside-out patch recordings as well as averaged mEPSCs from acute slices of the striatum prior to analysis to improve the quality of exponential fits. Electrophysiological recordings of striatal MSNs in acute coronal slices were performed with an external solution containing (in mM): 119 NaCl, 2.5 KCl, 2.5 $CaCl_2$, 1.3 $MgSO_4$, 1 NaH_2PO_4, 26.2 $NaHCO_3$ and 11 D-glucose (all from Sigma) and an internal solution containing (in mM): 115 $CsMeSO_4$, 20 $CsCl_2$, 10 HEPES, 2.5 $MgCl_2$, 4 NaATP, 0.4 NaGTP and 0.6 EGTA (all Sigma) (pH 7.2). 100 μM picrotoxin (Sigma) was included in the bath to block GABAergic IPSCs, and 0.5 μM TTX (Ascent Scientific, Tocris or Sigma) to prevent action potential-evoked EPSCs. In some recordings, 100 μM D-APV (Tocris) was included to block NMDARs, but did not significantly affect the decay times of mEPSCs at either age range recorded (P5–P6 and P14–P16), so data was pooled from recordings performed with and without D-APV. mEPSCs were evoked by the local application of 200 mM sucrose (Sigma) dissolved in external solution. Pipette resistances for these experiments were typically ~3–5 MΩ and series resistances ~15–20 MΩ. Only recording epochs in which series and input resistances varied less than 10% were analyzed. Monosodium glutamate was obtained from Sigma, kainic acid from Ascent Scientific or Tocris, TCM from Sigma, CTZ from Ascent Scientific or A.G. Scientific, and PEPA from Sigma.

Data Analysis

Average currents obtained from the outside-out patch and granule cell mEPSC experiments were best fit by a double exponential function with the form

$$I(t) = I_0 + A_{fast} e\left(\frac{t}{\tau_{fast}}\right) + A_{slow} e\left(\frac{t}{\tau_{slow}}\right).$$ To simplify the comparison of decay times across conditions, a single weighted decay measure was calculated from the area under the peak-

normalized current (Cathala et al., 2005), according to $\tau_{decay} = \frac{1}{I_{peak}} \int_{t_{peak}}^{t_0} I(t)dt$, where t_0 was 20 ms after the peak for patch deactivation, 60 ms for patch desensitization, and 60 ms for granule cell mEPSCs. The decay times of individual granule cell mEPSCs were also calculated in this manner, and the cumulative probability distributions shown reflect this weighted decay measure. For this purpose, individual mEPSCs were detected automatically using custom software in Igor Pro (Wavemetrics) and then manually screened for events that did not contain "contaminating" noise or additional mEPSCs during the 60 ms after the peak, and analysis was limited to these "clean" events. For mEPSCs recorded from MSNs in acute slices of the striatum, individual and average mEPSCs were well fit by a single exponential function, so cumulative probability distributions shown for these experiments reflect decay times obtained directly from single exponential fits rather than the weighted decay measure. Rise times reported for outside-out patch experiments were calculated by measuring the 20%–80% rise time, while cumulative probability distributions of rise times for mEPSCs reflect the 10%–90% rise time measured from individual mEPSCs. For comparisons of probability distributions, statistics were computed with a Kolmogorov-Smirnov test with a threshold of $p = 0.05$. For comparisons of mean values across multiple conditions, statistics were computed first with a Kruskal-Wallis test with a threshold of $p = 0.05$, and experiments containing significant differences were further evaluated using Wilcoxon posthoc tests where the threshold $\alpha = 0.05$ was adjusted by dividing α by the number of pairwise comparisons.

Computer Modeling

The kinetic model of AMPAR gating presented here was based on a model proposed in a recent report (Zhang et al., 2006). The functions describing the model were implemented using SCoP, a software package by Simulation Resource, Inc. Initial parameters were based on those reported by (Zhang et al., 2006) for GluR2, with some modifications based on a similar model of GluR1 (Robert and Howe, 2003). A least-square optimization algorithm was then performed in ScoP to fit the various parameters to the deactivation and desensitization data we obtained in our outside-out patch recordings containing GluR1 with or without the TARPs γ-2 and γ-4.

Supplementary Material

Refer to Web version on PubMed Central for supplementary material.

Acknowledgments

References

Andrasfalvy BK, Smith MA, Borchardt T, Sprengel R, Magee JC. Impaired regulation of synaptic strength in hippocampal neurons from GluR1-deficient mice. J Physiol. 2003; 552:35–45. [PubMed: 12878757]

Armstrong N, Gouaux E. Mechanisms for activation and antagonism of an AMPA-sensitive glutamate receptor: crystal structures of the GluR2 ligand binding core. Neuron. 2000; 28:165–181. [PubMed: 11086992]

Barbour B, Hausser M. Intersynaptic diffusion of neurotransmitter. Trends Neurosci. 1997; 20:377–384. [PubMed: 9292962]

Bats C, Groc L, Choquet D. The interaction between Stargazin and PSD-95 regulates AMPA receptor surface trafficking. Neuron. 2007; 53:719–734. [PubMed: 17329211]

Beique JC, Lin DT, Kang MG, Aizawa H, Takamiya K, Huganir RL. Synapse-specific regulation of AMPA receptor function by PSD-95. Proc Natl Acad Sci U S A. 2006; 103:19535–19540. [PubMed: 17148601]

Bredt DS, Nicoll RA. AMPA receptor trafficking at excitatory synapses. Neuron. 2003; 40:361–379. [PubMed: 14556714]

Canti C, Davies A, Berrow NS, Butcher AJ, Page KM, Dolphin AC. Evidence for two concentration-dependent processes for beta-subunit effects on alpha1B calcium channels. Biophys J. 2001; 81:1439–1451. [PubMed: 11509358]

Cathala L, Holderith NB, Nusser Z, DiGregorio DA, Cull-Candy SG. Changes in synaptic structure underlie the developmental speeding of AMPA receptor-mediated EPSCs. Nat Neurosci. 2005; 8:1310–1318. [PubMed: 16172604]

Chen L, Chetkovich DM, Petralia RS, Sweeney NT, Kawasaki Y, Wenthold RJ, Bredt DS, Nicoll RA. Stargazin regulates synaptic targeting of AMPA receptors by two distinct mechanisms. Nature. 2000; 408:936–943. [PubMed: 11140673]

Clements JD. Transmitter timecourse in the synaptic cleft: its role in central synaptic function. Trends Neurosci. 1996; 19:163–171. [PubMed: 8723198]

Clements JD, Feltz A, Sahara Y, Westbrook GL. Activation kinetics of AMPA receptor channels reveal the number of functional agonist binding sites. J Neurosci. 1998; 18:119–127. [PubMed: 9412492]

Coleman SK, Moykkynen T, Cai C, von Ossowski L, Kuismanen E, Korpi ER, Keinanen K. Isoform-specific early trafficking of AMPA receptor flip and flop variants. J Neurosci. 2006; 26:11220–11229. [PubMed: 17065461]

Diamond JS. Neuronal glutamate transporters limit activation of NMDA receptors by neurotransmitter spillover on CA1 pyramidal cells. J Neurosci. 2001; 21:8328–8338. [PubMed: 11606620]

Elias GM, Funke L, Stein V, Grant SG, Bredt DS, Nicoll RA. Synapse-Specific and Developmentally Regulated Targeting of AMPA Receptors by a Family of MAGUK Scaffolding Proteins. Neuron. 2006; 52:307–320. [PubMed: 17046693]

Fukaya M, Tsujita M, Yamazaki M, Kushiya E, Abe M, Akashi K, Natsume R, Kano M, Kamiya H, Watanabe M, Sakimura K. Abundant distribution of TARP gamma-8 in synaptic and extrasynaptic surface of hippocampal neurons and its major role in AMPA receptor expression on spines and dendrites. Eur J Neurosci. 2006; 24:2177–2190. [PubMed: 17074043]

Fukaya M, Yamazaki M, Sakimura K, Watanabe M. Spatial diversity in gene expression for VDCCgamma subunit family in developing and adult mouse brains. Neurosci Res. 2005

Hansen KB, Yuan H, Traynelis SF. Structural aspects of AMPA receptor activation, desensitization and deactivation. Curr Opin Neurobiol. 2007

Hashimoto K, Fukaya M, Qiao X, Sakimura K, Watanabe M, Kano M. Impairment of AMPA receptor function in cerebellar granule cells of ataxic mutant mouse stargazer. J Neurosci. 1999; 19:6027–6036. [PubMed: 10407040]

Hausser M, Clark BA. Tonic synaptic inhibition modulates neuronal output pattern and spatiotemporal synaptic integration. Neuron. 1997; 19:665–678. [PubMed: 9331356]

Horning MS, Mayer ML. Regulation of AMPA receptor gating by ligand binding core dimers. Neuron. 2004; 41:379–388. [PubMed: 14766177]

Jonas P. The Time Course of Signaling at Central Glutamatergic Synapses. News Physiol Sci. 2000; 15:83–89. [PubMed: 11390884]

Kampa BM, Clements J, Jonas P, Stuart GJ. Kinetics of Mg2+ unblock of NMDA receptors: implications for spike-timing dependent synaptic plasticity. J Physiol. 2004; 556:337–345. [PubMed: 14754998]

Kato AS, Zhou W, Milstein AD, Knierman MD, Siuda ER, Dotzlaf JE, Yu H, Hale JE, Nisenbaum ES, Nicoll RA, Bredt DS. New transmembrane AMPA receptor regulatory protein isoform, gamma-7, differentially regulates AMPA receptors. J Neurosci. 2007; 27:4969–4977. [PubMed: 17475805]

Koike M, Tsukada S, Tsuzuki K, Kijima H, Ozawa S. Regulation of kinetic properties of GluR2 AMPA receptor channels by alternative splicing. J Neurosci. 2000; 20:2166–2174. [PubMed: 10704491]

Korber C, Werner M, Kott S, Ma ZL, Hollmann M. The transmembrane AMPA receptor regulatory protein gamma4 is a more effective modulator of AMPA receptor function than stargazin (gamma2). J Neurosci. 2007; 27:8442–8447. [PubMed: 17670991]

Kott S, Werner M, Korber C, Hollmann M. Electrophysiological properties of AMPA receptors are differentially modulated depending on the associated member of the TARP family. J Neurosci. 2007; 27:3780–3789. [PubMed: 17409242]

Kullmann DM, Min MY, Asztely F, Rusakov DA. Extracellular glutamate diffusion determines the occupancy of glutamate receptors at CA1 synapses in the hippocampus. Philos Trans R Soc Lond B Biol Sci. 1999; 354:395–402. [PubMed: 10212489]

Lester RA, Jahr CE. NMDA channel behavior depends on agonist affinity. J Neurosci. 1992; 12:635–643. [PubMed: 1346806]

Magee JC, Cook EP. Somatic EPSP amplitude is independent of synapse location in hippocampal pyramidal neurons. Nat Neurosci. 2000; 3:895–903. [PubMed: 10966620]

Malinow R, Malenka RC. AMPA receptor trafficking and synaptic plasticity. Annu Rev Neurosci. 2002; 25:103–126. [PubMed: 12052905]

Mosbacher J, Schoepfer R, Monyer H, Burnashev N, Seeburg PH, Ruppersberg JP. A molecular determinant for submillisecond desensitization in glutamate receptors. Science. 1994; 266:1059–1062. [PubMed: 7973663]

Nakagawa T, Cheng Y, Ramm E, Sheng M, Walz T. Structure and different conformational states of native AMPA receptor complexes. Nature. 2005; 433:545–549. [PubMed: 15690046]

Nicoll RA, Tomita S, Bredt DS. Auxiliary subunits assist AMPA-type glutamate receptors. Science. 2006; 311:1253–1256. [PubMed: 16513974]

Osten P, Stern-Bach Y. Learning from stargazin: the mouse, the phenotype and the unexpected. Curr Opin Neurobiol. 2006; 16:275–280. [PubMed: 16678401]

Overstreet LS, Kinney GA, Liu YB, Billups D, Slater NT. Glutamate transporters contribute to the time course of synaptic transmission in cerebellar granule cells. J Neurosci. 1999; 19:9663–9673. [PubMed: 10531468]

Pan ZZ, Tong G, Jahr CE. A false transmitter at excitatory synapses. Neuron. 1993; 11:85–91. [PubMed: 8101712]

Priel A, Kolleker A, Ayalon G, Gillor M, Osten P, Stern-Bach Y. Stargazin reduces desensitization and slows deactivation of the AMPA-type glutamate receptors. J Neurosci. 2005; 25:2682–2686. [PubMed: 15758178]

Raman IM, Trussell LO. The mechanism of alpha-amino-3-hydroxy-5-methyl-4-isoxazolepropionate receptor desensitization after removal of glutamate. Biophys J. 1995; 68:137–146. [PubMed: 7711235]

Robert A, Armstrong N, Gouaux JE, Howe JR. AMPA receptor binding cleft mutations that alter affinity, efficacy, and recovery from desensitization. J Neurosci. 2005; 25:3752–3762. [PubMed: 15829627]

Robert A, Howe JR. How AMPA receptor desensitization depends on receptor occupancy. J Neurosci. 2003; 23:847–858. [PubMed: 12574413]

Rouach N, Byrd K, Petralia RS, Elias GM, Adesnik H, Tomita S, Karimzadegan S, Kealey C, Bredt DS, Nicoll RA. TARP gamma-8 controls hippocampal AMPA receptor number, distribution and synaptic plasticity. Nat Neurosci. 2005; 8:1525–1533. [PubMed: 16222232]

Sargent PB, Saviane C, Nielsen TA, DiGregorio DA, Silver RA. Rapid vesicular release, quantal variability, and spillover contribute to the precision and reliability of transmission at a glomerular synapse. J Neurosci. 2005; 25:8173–8187. [PubMed: 16148225]

Schnell E, Sizemore M, Karimzadegan S, Chen L, Bredt DS, Nicoll RA. Direct interactions between PSD-95 and stargazin control synaptic AMPA receptor number. Proc Natl Acad Sci U S A. 2002; 99:13902–13907. [PubMed: 12359873]

Sekiguchi M, Takeo J, Harada T, Morimoto T, Kudo Y, Yamashita S, Kohsaka S, Wada K. Pharmacological detection of AMPA receptor heterogeneity by use of two allosteric potentiators in rat hippocampal cultures. Br J Pharmacol. 1998; 123:1294–1303. [PubMed: 9579722]

Shaner NC, Campbell RE, Steinbach PA, Giepmans BN, Palmer AE, Tsien RY. Improved monomeric red, orange and yellow fluorescent proteins derived from Discosoma sp. red fluorescent protein. Nat Biotechnol. 2004; 22:1567–1572. [PubMed: 15558047]

Sheng M, Kim MJ. Postsynaptic signaling and plasticity mechanisms. Science. 2002; 298:776–780. [PubMed: 12399578]

Silver RA, Colquhoun D, Cull-Candy SG, Edmonds B. Deactivation and desensitization of non-NMDA receptors in patches and the time course of EPSCs in rat cerebellar granule cells. J Physiol. 1996; 493(Pt 1):167–173. [PubMed: 8735702]

Sun Y, Olson R, Horning M, Armstrong N, Mayer M, Gouaux E. Mechanism of glutamate receptor desensitization. Nature. 2002; 417:245–253. [PubMed: 12015593]

Swanson GT, Kamboj SK, Cull-Candy SG. Single-channel properties of recombinant AMPA receptors depend on RNA editing, splice variation, and subunit composition. J Neurosci. 1997; 17:58–69. [PubMed: 8987736]

Takahashi T. Postsynaptic receptor mechanisms underlying developmental speeding of synaptic transmission. Neurosci Res. 2005; 53:229–240. [PubMed: 16219377]

Tomita S, Adesnik H, Sekiguchi M, Zhang W, Wada K, Howe JR, Nicoll RA, Bredt DS. Stargazin modulates AMPA receptor gating and trafficking by distinct domains. Nature. 2005; 435:1052–1058. [PubMed: 15858532]

Tomita S, Chen L, Kawasaki Y, Petralia RS, Wenthold RJ, Nicoll RA, Bredt DS. Functional studies and distribution define a family of transmembrane AMPA receptor regulatory proteins. J Cell Biol. 2003; 161:805–816. [PubMed: 12771129]

Tomita S, Fukata M, Nicoll RA, Bredt DS. Dynamic interaction of stargazin-like TARPs with cycling AMPA receptors at synapses. Science. 2004; 303:1508–1511. [PubMed: 15001777]

Turetsky D, Garringer E, Patneau DK. Stargazin modulates native AMPA receptor functional properties by two distinct mechanisms. J Neurosci. 2005; 25:7438–7448. [PubMed: 16093395]

Vorobjev VS, Sharonova IN, Haas HL, Sergeeva OA. Differential modulation of AMPA receptors by cyclothiazide in two types of striatal neurons. Eur J Neurosci. 2000; 12:2871–2880. [PubMed: 10971630]

Wall MJ, Robert A, Howe JR, Usowicz MM. The speeding of EPSC kinetics during maturation of a central synapse. Eur J Neurosci. 2002; 15:785–797. [PubMed: 11906520]

Wang YW, Ding JP, Xia XM, Lingle CJ. Consequences of the stoichiometry of Slo1 alpha and auxiliary beta subunits on functional properties of large-conductance Ca2+-activated K+ channels. J Neurosci. 2002; 22:1550–1561. [PubMed: 11880485]

Xu-Friedman MA, Regehr WG. Ultrastructural contributions to desensitization at cerebellar mossy fiber to granule cell synapses. J Neurosci. 2003; 23:2182–2192. [PubMed: 12657677]

Zhang W, Robert A, Vogensen SB, Howe JR. The relationship between agonist potency and AMPA receptor kinetics. Biophys J. 2006; 91:1336–1346. [PubMed: 16731549]

Ziff EB. TARPs and the AMPA Receptor Trafficking Paradox. Neuron. 2007; 53:627–633. [PubMed: 17329203]
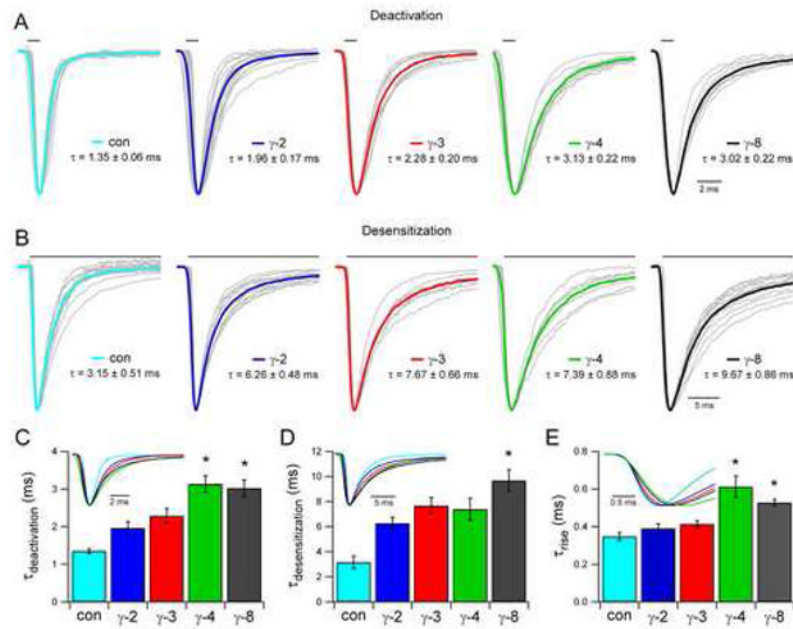
Figure 1. TARP Subtype Determines the Kinetics of GluR1 in HEK293T Cells
(A and B) Average responses of outside-out patches to 1 ms (A) or 100 ms (B) applications of 1 mM glutamate are normalized and aligned to the peak. Superimposed responses of individual patches are displayed in grey, and averages across experiments are shown in color. Weighted time constant values calculated from the area under the peak-normalized response are displayed as mean ± SEM (see Experimental Procedures).

(C) The time course of deactivation is quantified (mean ± SEM), and the average traces across conditions from (A) are superimposed (inset). All TARPs slowed deactivation of GluR1 (flip) (control: n = 11; γ-2: n = 16, p < 0.005; γ-3: n = 9, p < 0.0002; γ-4: n = 8, p < 0.0001; γ-8: n = 8, p < 0.0001), and some TARPs further slowed deactivation of GluR1 relative to γ-2, as indicated by asterisks (γ-4: p < 0.001; γ-8: p < 0.003).

(D) The time course of desensitization is quantified (mean ± SEM), and the average traces across conditions from (B) are superimposed (inset). All TARPs slowed desensitization of GluR1 (control: n = 14; γ-2: n = 12, p < 0.0003; γ-3: n = 9, p < 0.0003; γ-4: n = 8, p < 0.002; γ-8: n = 13, p < 0.0001), while TARP γ-8 further slowed desensitization of GluR1 relative to γ-2, as indicated by the asterisk (p < 0.002).

(E) The rise time course in response to 1 ms applications of glutamate is quantified (mean ± SEM), and the average traces across conditions from (A) are aligned to the 10% rise point and superimposed (inset). Some TARPs slowed activation of GluR1, as indicated by asterisks (γ-4: p < 0.0004; γ-8: p < 0.0006).
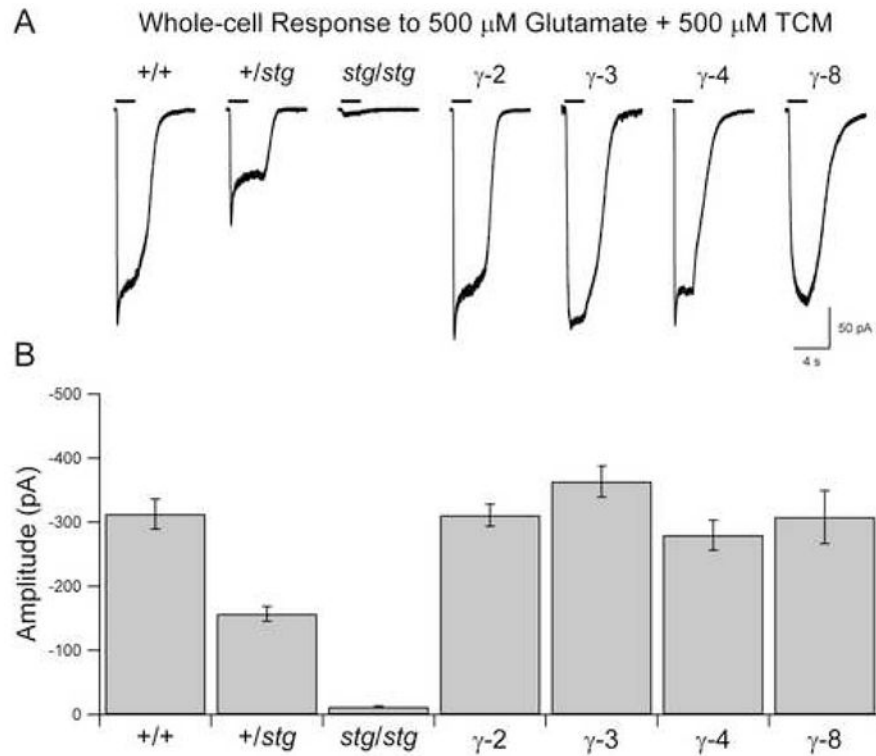
Figure 2. Surface AMPAR Expression in Cerebellar Granule Neurons
(A) Representative whole-cell responses to the local application of 500 μM glutamate + 500 μM trichloromethiazide (TCM), which blocks AMPAR desensitization, demonstrate that ectopic TARP expression rescues surface AMPAR responses in *stg/stg* granule neurons.
(B) Whole-cell responses are quantified. All TARP subtypes rescued surface AMPAR responses in *stg/stg* granule neurons to wild type levels (*stg/stg*: n = 25; γ-2: n = 29; γ-3: n = 24; γ-4: n = 20; γ-8: n = 17; Wilcoxon tests, $p < 0.0001$). Responses were reduced in *+/stg* neurons (n = 20) compared to +/+ (n = 15), $p < 0.0001$.
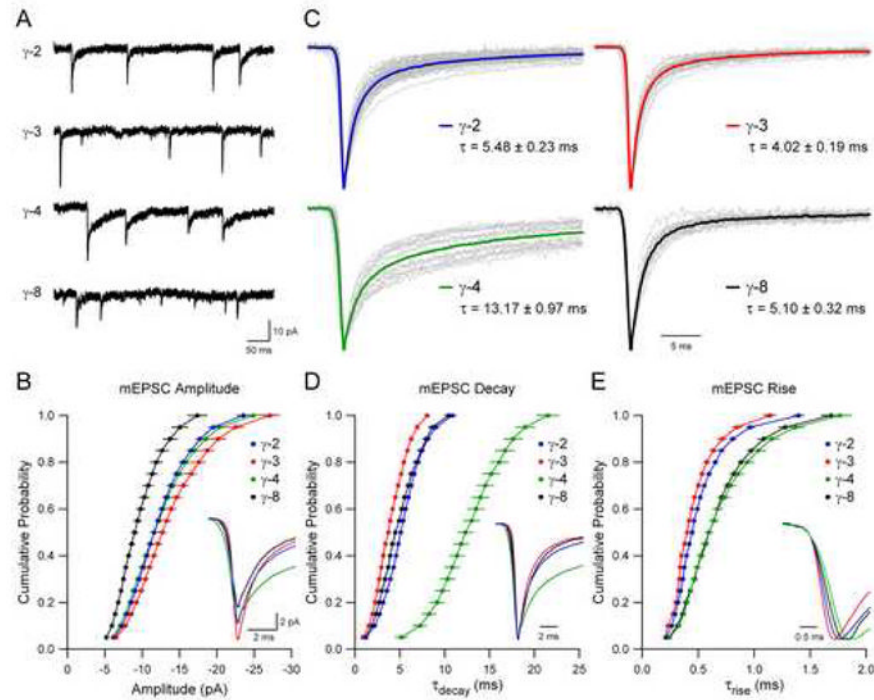
Figure 3. TARP Subtype Controls Synaptic AMPA Receptor Gating

(A) Sample records demonstrate that each TARP subtype is sufficient to restore the synaptic localization of native AMPARs in *stg/stg* granule neurons.

(B) mEPSC amplitude depends on TARP subtype (Kolmogorov-Smirnov comparisons to γ-2: n = 40; γ-3: n = 25, p < 0.007; γ-4: n = 18, n.s.; γ-8: n = 14, p < 0.001). Cumulative distributions are displayed as mean ± SEM, and averages of mEPSCs are aligned to the peak and superimposed (inset).

(C) Average mEPSCs are normalized and aligned to the peak. Average mEPSCs from individual neurons are displayed in grey, and averages of all experiments for each condition are shown in color. Weighted time constant values calculated from the area under the peak-normalized current are displayed as mean ± SEM (see Experimental Procedures).

(D) mEPSC decay depends on TARP subtype (Kolmogorov-Smirnov comparisons to γ-2; γ-3: p < 0.001; γ-4: p < 0.001; γ-8: n.s.). Cumulative distributions are displayed as mean ± SEM, and average mEPSCs across conditions from (C) are aligned to the peak and superimposed (inset).

(E) mEPSC rise depends on TARP subtype (Kolmogorov-Smirnov comparisons to γ-2; γ-3: p < 0.001; γ-4: p < 0.001; γ-8: p < 0.001). Cumulative distributions are displayed as mean ± SEM, and average mEPSCs across conditions from (C) are aligned to the 10% rise point and superimposed (inset).
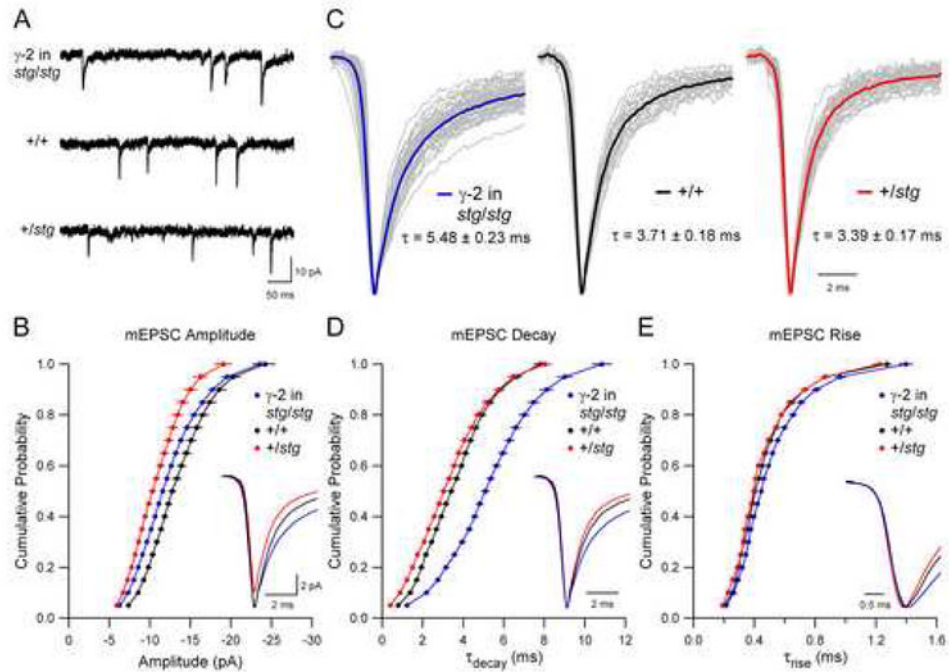
Figure 4. TARPs Dose-Dependently Control Synaptic AMPA Receptor Gating

(A) Sample records demonstrate that characteristics of quantal synaptic AMPAR currents vary with the expression level of γ-2.

(B) mEPSC amplitude depends on TARP expression level (Kolmogorov-Smirnov comparisons to wild type (+/+): n = 22; +/*stg*: n = 28, p < 0.001; γ-2 in *stg*/*stg*: n = 40, p < 0.001). Cumulative distributions are displayed as mean ± SEM, and averages of mEPSCs are aligned to the peak and superimposed (inset).

(C) Average mEPSCs are normalized and aligned to the peak. Average mEPSCs from individual neurons are displayed in grey, and averages of all experiments for each condition are shown in color (γ-2 in *stg*/*stg* data from Figure 3C is replotted on a different timescale for comparison). Weighted time constant values calculated from the area under the peak-normalized current are displayed as mean ± SEM (see Experimental Procedures).

(D) mEPSC decay depends on TARP expression level (Kolmogorov-Smirnov comparisons to wild type (+/+); +/*stg*: p < 0.004; γ-2 in *stg*/*stg*: p < 0.001). Cumulative distributions are displayed as mean ± SEM, and average mEPSCs across conditions from (C) are aligned to the peak and superimposed (inset).

(E) mEPSC rise is independent of TARP expression level (Kolmogorov-Smirnov comparisons to wild type (+/+); +/*stg*: n.s.; γ-2 in *stg*/*stg*: n.s.). Cumulative distributions are displayed as mean ± SEM, and average mEPSCs across conditions from (C) are aligned to the 10% rise point and superimposed (inset).
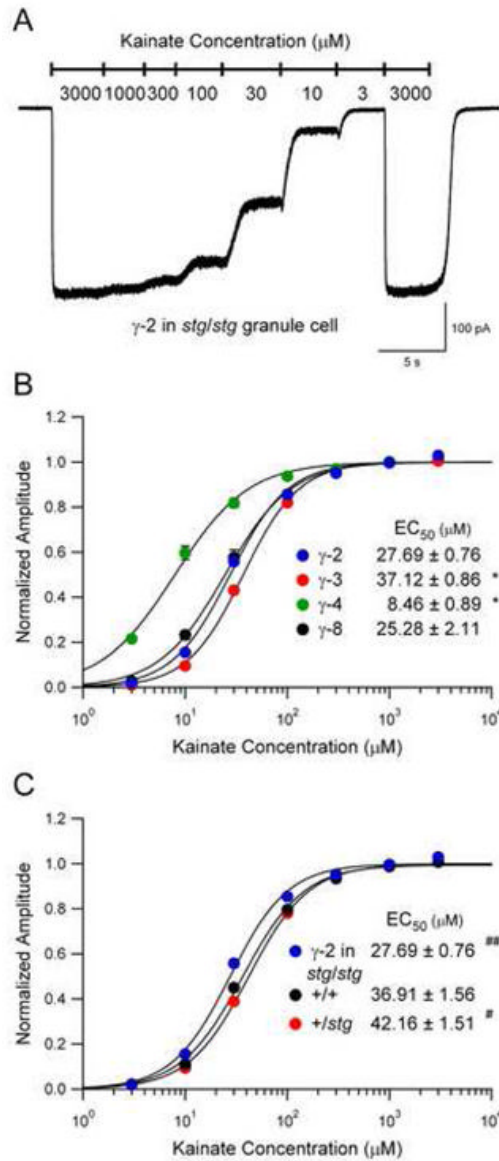
Figure 5. AMPAR Agonist Dose-Response Relationship Depends on TARP Subtype and Expression Level

(A) Example of a typical experiment in which different concentrations of kainate were applied via a local perfusion barrel to an *stg/stg* granule neuron expressing γ-2. Saturating concentration (3 mM) was applied at the start and finish of the concentration ladder to exclude the possibility of run-down.

(B) AMPAR affinity for kainate depends on TARP subtype. EC_{50} values are displayed as mean ± SEM for γ-2: n = 8; γ-3: n = 12; γ-4: n = 12; γ-8: n = 7. Asterisks indicate statistical significance relative to TARP γ-2 (* $p < 0.0001$).

(C) AMPAR affinity for kainate depends on TARP expression level. EC_{50} values are displayed as mean ± SEM for wild type (+/+): n = 12; +/*stg*: n = 12; γ-2 in *stg/stg*: n = 12. Symbols indicate statistical significance relative to wild type (+/+) ([#] $p < 0.03$, [##] $p < 0.001$).
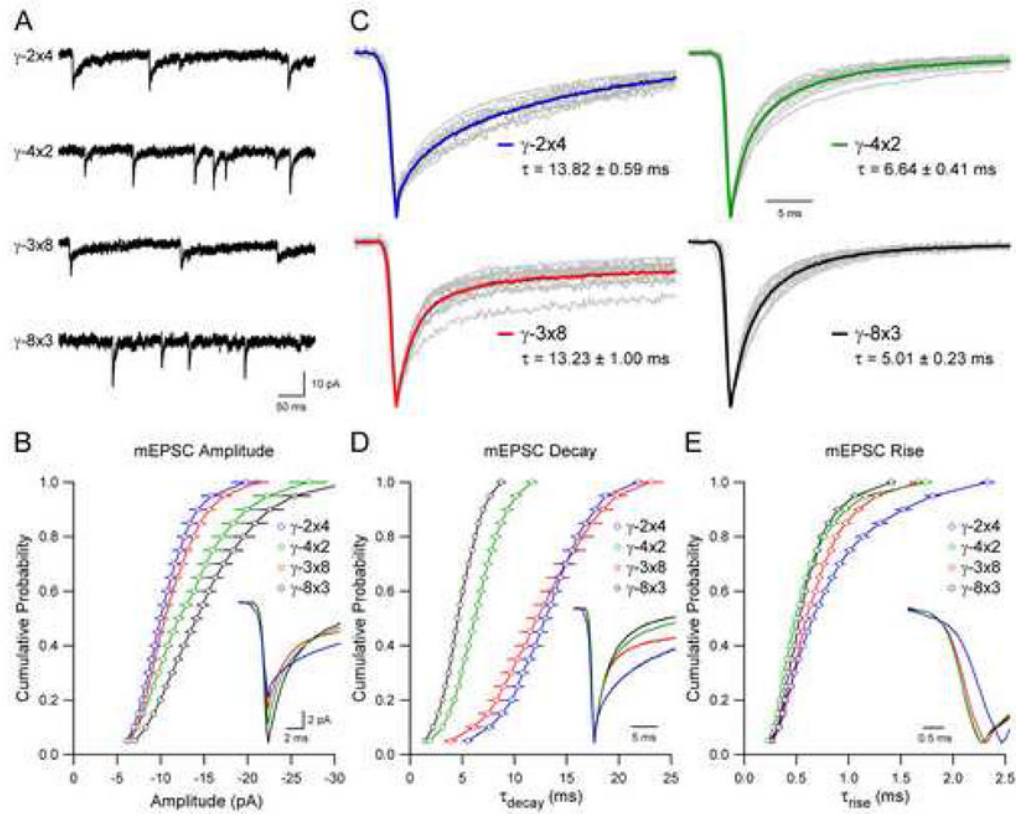
Figure 6. First Extracellular Domain Mediates TARP Subtype-Specific Gating of AMPA Receptors

(A) Sample records demonstrate that chimeric TARPs in which the extracellular domain (Ex1) of γ-2 and γ-4 are swapped (γ-2×4 and γ-4×2) or the Ex1 of γ-3 and γ-8 are swapped (γ-3×8 and γ-8×3) are able to restore the synaptic localization of native AMPARs in *stg/stg* granule neurons.

(B) mEPSC amplitude depends on TARP Ex1 (Kolmogorov-Smirnov tests, γ-2×4: n = 11 vs. γ-4×2: n = 14, p < 0.001; γ-3×8: n = 13 vs. γ-8×3: n = 14, p < 0.001). Cumulative distributions are displayed as mean ± SEM, and averages of mEPSCs are aligned to the peak and superimposed (inset).

(C) Average mEPSCs are normalized and aligned to the peak. Average mEPSCs from individual neurons are displayed in grey, and averages of all experiments for each condition are shown in color. Weighted time constant values calculated from the area under the peak-normalized current are displayed as mean ± SEM (see Experimental Procedures).

(D) mEPSC decay depends on TARP Ex1 (Kolmogorov-Smirnov tests, γ-2×4 vs. γ-4×2, p < 0.001; γ-3×8 vs. γ-8×3, p < 0.001). Cumulative distributions are displayed as mean ± SEM, and average mEPSCs across conditions from (C) are aligned to the peak and superimposed (inset).

(E) mEPSC rise depends on TARP Ex1 (Kolmogorov-Smirnov tests, γ-2×4 vs. γ-4×2, p < 0.001; γ-3×8 vs. γ-8×3, p = 0.008). Cumulative distributions are displayed as mean ± SEM, and average mEPSCs across conditions from (C) are aligned to the 10% rise point and superimposed (inset).
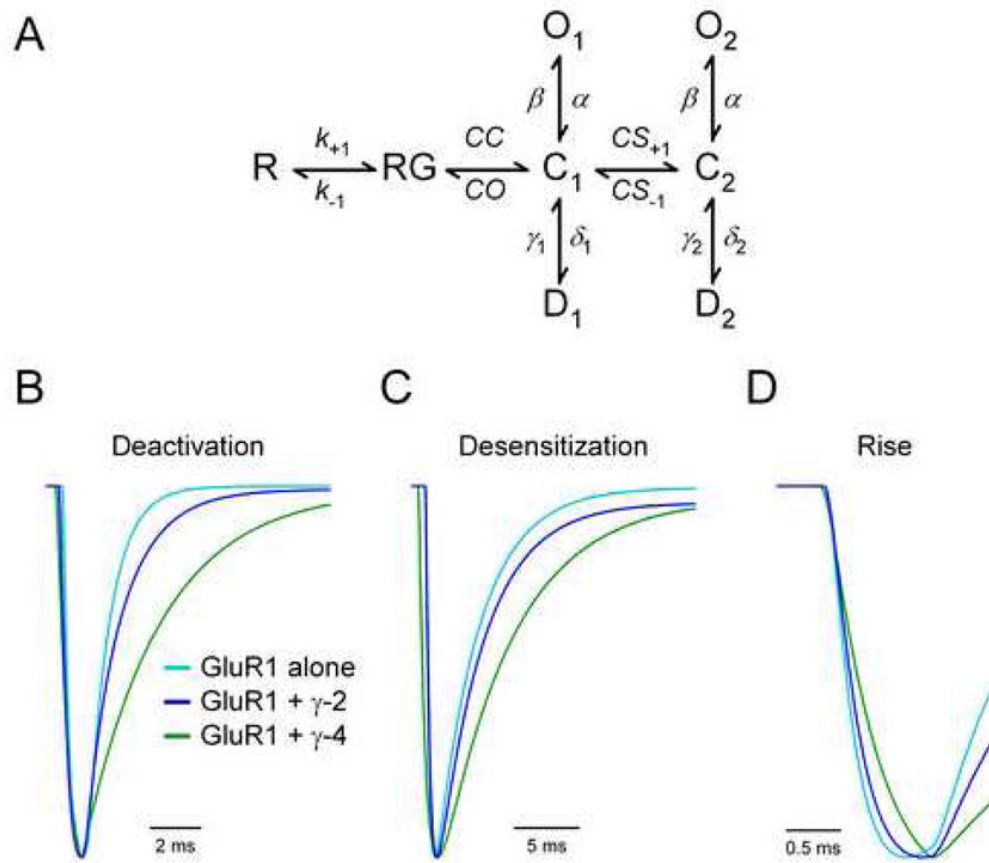
Figure 7. A Simple Kinetic Model of TARP Control of AMPAR Gating

(A) Diagram illustrating the kinetic scheme used to model the response of AMPAR channels to brief pulses of glutamate.

(B) Simulated responses of GluR1 alone, GluR1 + γ-2 and GluR1 + γ-4 to a 1 ms square pulse of glutamate. Traces are scaled and aligned to the peak to illustrate the time course of deactivation.

(C) Simulated responses of GluR1 alone, GluR1 + γ-2 and GluR1 + γ-4 to a 100 ms square pulse of glutamate. Traces are scaled and aligned to the peak to illustrate the time course of desensitization.

(D) Simulated responses of GluR1 alone, GluR1 + γ-2 and GluR1 + γ-4 to a 1 ms square pulse of glutamate from (B) are aligned to the 10% rise point to illustrate the time course of activation.
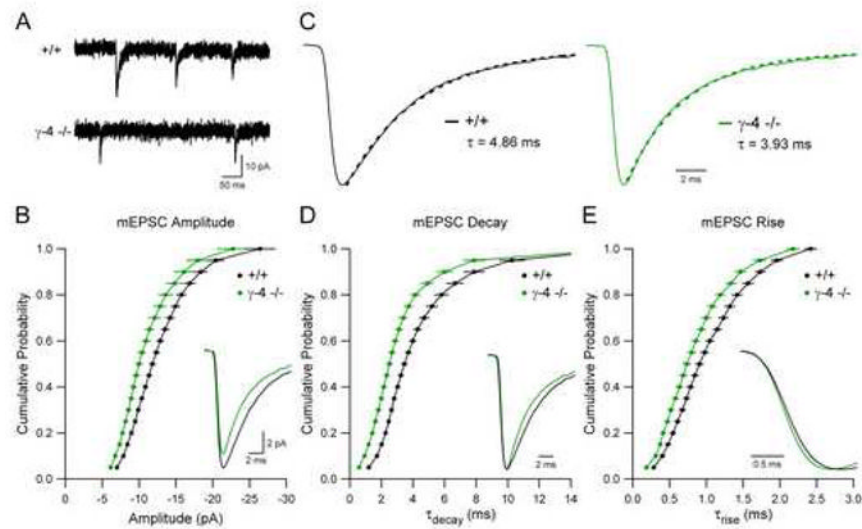
Figure 8. Deficits in Synaptic AMPAR Function in Striatum of Neonatal TARP γ-4 Knockout Mice

(A) Sample records demonstrate that quantal synaptic AMPAR transmission is altered in MSNs in the neonatal (P5–P6) striatum in γ-4 −/− mice.

(B) mEPSC amplitude is reduced in γ-4 −/− mice (Kolmogorov-Smirnov test, +/+: n = 22 vs. γ-4 −/−: n = 22, $p < 0.001$). Cumulative distributions are displayed as mean ± SEM, and representative averaged mEPSCs are aligned to the peak and superimposed (inset).

(C) Representative averaged mEPSCs are normalized to the peak (solid lines), and the decay phase is fit with a single exponential function (broken lines). The corresponding decay time constant values are displayed.

(D) mEPSC decay is accelerated in γ-4 −/− mice (Kolmogorov-Smirnov test, $p < 0.001$). Cumulative distributions are displayed as mean ± SEM, and the representative averaged mEPSCs from (C) are aligned to the peak and superimposed (inset).

(E) mEPSCs rise is accelerated in γ-4 −/− mice (Kolmogorov-Smirnov test, $p < 0.001$). Cumulative distributions are displayed as mean ± SEM, and the representative averaged mEPSCs from (C) are aligned to the 10% rise point and superimposed (inset).

Table 1

Parameters for Kinetic Model of Regulation of AMPARs by TARPs

	GluR1 alone	GluR1 + γ-2	GluR1 + γ-4
α	$6000\ s^{-1}$		
β	$10000\ s^{-1}$		
k_{+1}	$1\times10^7\ M^{-1}s^{-1}$		
k_{-1}	$5\times10^4\ s^{-1}$		
CC	$36500\ s^{-1}$	$25000\ s^{-1}$	$12500\ s^{-1}$
CO	$4550\ s^{-1}$	$2500\ s^{-1}$	$1750\ s^{-1}$
CS_{+1}	$300\ s^{-1}$	$1000\ s^{-1}$	$10000\ s^{-1}$
CS_{-1}	$10000\ s^{-1}$	$3400\ s^{-1}$	$4200\ s^{-1}$
δ_1	$1100\ s^{-1}$		
γ_1	$1\ s^{-1}$	$10\ s^{-1}$	
δ_2	$300\ s^{-1}$		
γ_2	$10\ s^{-1}$		
$\tau_{deactivation}$	1.15 ms	1.73 ms	3.31 ms
$\tau_{desensitization}$	3.77 ms	6.37 ms	7.71 ms
τ_{rise}	0.26 ms	0.30 ms	0.46 ms

The rate constants refer to the model depicted in Figure 7A. When values are omitted in the table, the corresponding value for GluR1 alone was used. $\tau_{deactivation}$ and $\tau_{desensitization}$ were calculated from the simulated current traces shown in Figure 7B and 7C by measuring the area under the peak-normalized curve (see Experimental Procedures), while τ_{rise} was calculated by measuring the 20%–80% rise time of the simulated traces shown in Figure 7D.